Modern Physics Letters B
Vol. 33, No. 7 (2019) 1950077 (18 pages)

DOI: 10.1142/S0217984919500775

Optimization of neon soft X-ray yield in a low-energy dense plasma focus device

M. A. Malek*

Department of Physics, Jahangirnagar University,
Savar, Dhaka 1342, Bangladesh
Physics Discipline, Khulna University, Khulna 9208, Bangladesh
malekphy@gmail.com

M. K. Islam

Plasma Physics Division, Atomic Energy Centre,
Bangladesh Atomic Energy Commission, Ramna, Dhaka 1000, Bangladesh
khairulislam@yahoo.com

M. Akel

Department of Physics, Atomic Energy Commission,
P. O. Box 6091, Damascus, Syria

M. Salahuddin

Department of Physics, Jahangirnagar University,
Savar, Dhaka 1342, Bangladesh

S. H. Saw[†,‡] and S. Lee[‡,§,¶]

[†] *Nilai University, No. 1, Persiaran Universiti,*
Putra Nilai, Bandar Baru Nilai, 71800 Nilai, Negeri Sembilan, Malaysia
[‡] *Institute for Plasma Focus Studies,*
32 Oakpark Drive, Chadstone, VIC 3148, Australia
[§] *INTI International University, Persiaran Perdana BBN,*
Putra Nilai, 71800 Nilai, Negeri Sembilan, Malaysia
[¶] *University of Malaya, 50603 Kuala Lumpur, Malaysia*

Received 3 December 2018
Accepted 26 December 2018
Published 11 March 2019

The modified version of Lee model code is used in numerical experiments for characterizing and optimizing neon soft X-ray yield ($Y_{\rm sxr}$) of the United Nations University/International Center for Theoretical Physics Plasma Focus Facility (UNU/ICTP PFF) device operated at 14 kV and 30 μF. In our present work, the neon yield $Y_{\rm sxr}$ is improved with an optimized UNU/ICTP PFF device by computing the

*Corresponding author.

optimum combination of static inductance (L_0), anode length (z_0), anode radius (a) and cathode radius (b), keeping fixed their ratio ($c = b/a$) at 3.368, through a lot of numerical experiments at six operating pressures (P_0). At lower P_0 (e.g. 2.0, 2.5 and 3.3 Torr), the optimum L_0 value, together with the corresponding optimum combination of z_0, a and b, is found to be 15 nH, whereas at higher P_0 (e.g. 4.0, 5.0 and 6.0 Torr), it is obtained as 10 nH. Though the computed maximum neon yield $Y_{\rm sxr}$ (57.2 J with the corresponding efficiency of 1.94%) is found at $P_0 = 4.0$ Torr, assuming an achievable range of incorporating low-inductance technology, the best optimum combination of L_0, z_0, a and b is found to be at $P_0 = 3.3$ Torr, resulting in the computed optimum neon yield $Y_{\rm sxr}$ of 54.6 J with a corresponding efficiency of 1.9%. This computed neon yield $Y_{\rm sxr}$ is about 11 times higher than the measured value (5.4 ± 1 J) at optimum $P_0 = 3.0$ Torr of UNU/ICTP PFF. It is also observed that our computed neon yield $Y_{\rm sxr}$ is improved by around six times from the previously computed value, which was 9.5 J at the optimum $P_0 = 3.5$ Torr for optimum anode configuration of this machine. In addition, neon yield $Y_{\rm sxr}$ is obtained with our optimized combination of L_0, z_0, a and b at 11.5 kV and compared with the measured neon yield $Y_{\rm sxr}$ of the NX2 machine.

Keywords: Dense plasma focus; Lee model code; inductance; electrode geometry; neon soft X-ray.

1. Introduction

The dense plasma focus (DPF) device is a non-radioactive co-axial accelerator with relatively simple operating principle that produces a high-density, high-temperature plasma along with pulsed fusion neutron yield, soft and hard X-rays, high-energy electrons and ion beams and electromagnetic waves.[1–3] This device is easy to construct, requires minimum maintenance and cost. The pulsed X-ray emitted from it has the highest intensity among all other existing devices of equivalent operating energy.[4] The DPF device as a high-intensity pulsed X-ray source has a wide range of real-life applications such as in X-ray spectroscopy,[5] X-ray microscopy and lithography,[6] X-ray laser pumping,[7] X-ray crystallography,[8] X-ray radiography,[9] X-ray back-lighter[10] and X-ray micromachining.[11] The United Nations University/International Center for Theoretical Physics Plasma Focus Facility (UNU/ICTP PFF) is a 3.3-kJ Mather-type DPF machine which is switched by a parallel-plate cascade air gap, powered by a 15-kV and 30-μF Maxwell capacitor.[12] With support from the UNU and ICTP, the UNU Training Programme in Plasma and Laser Technology developed this device to initiate and promote practical knowledge and skills in plasma physics as well as fusion, in developing countries.[13] This machine produces realistic focusing action operating in several gases (He, Ne, Ar, H_2, CO_2, D_2, N_2, etc.).[12,14]

The neon yield $Y_{\rm sxr}$ for optimized DPF with operating energy in the range of 0.2 kJ–1 MJ was computed through numerical experiments by the Lee model code and it is observed that neon is a suitable operating gas for the device as a source of soft X-ray yield.[15] The Lee model code is used to compute the realistic focus parameters along with the soft X-ray yield by only adjusting the computed discharge current waveform with the experimentally measured current waveform. In the case of NX2 DPF machine, this code has been successfully used showing a reasonably good agreement between the computed and measured values of neon yield Y_{sxr} as a function of pressure.[4] Therefore, the Lee model code is used to compute and optimize a DPF machine for improving the realistic yield Y_{sxr}.

For enhancing X-ray yields from the DPF device, many efforts have been made by changing the bank, tube and operating parameters such as energy of the bank, static circuit inductance, discharge current, electrode configuration (shape and materials), insulator materials and dimensions, gas composition and gas pressure.[16] There is a combined drive parameter (speed factor) $(I_{\mathrm{peak}}/a)/\sqrt{\rho}$, in which I_{peak} is the peak discharge current and ρ is the ambient gas density, which is one of the most important parameters that determine the performance of a DPF as a source of different types of energetic particles and radiations. The drive parameter also known as the speed factor (SF) is a fundamental scaling parameter that determines the characteristic axial speed and characteristic radial speed of the plasma focus when correctly formulated as an electromagnetic device. The Mather-type DPF devices with a wide range of energies (E_0) from few kJ to hundreds of kJ operated in neutron-optimized regime have a remarkably constant drive parameter (89 ± 9) kA/(cm $\cdot$ Torr$^{0.5}$) when operated in deuterium.[17] The constancy of this parameter is related to the observation that in optimized devices the peak axial speed varies little from 10 cm/ms. This constancy of this parameter has been considered as a design tool of a DPF machine for neutron production in deuterium.[18–20] For a neon plasma focus designed for optimum yield of characteristic neon soft X-ray, the drive parameter plays a dominant role also, since the pinch plasma needs to be within a temperature window[15,18] required for the neon to be ionized to a combination of hydrogen-like and helium-like plasma. This places a requirement of on-axis radial shock speed and hence on the SF, although the requirement on the SF for neutron yield in deuterium and for characteristic soft X-ray yield will not necessarily be the same, due to the difference in the mechanisms of production of D-D neutrons and neon soft X-rays. Nevertheless a study of the range of drive parameters for good soft X-ray yields is useful and hence the values are also recorded in the present study.

The measured value of neon yield Y_{sxr} from UNU/ICTP PFF was (5.4 ± 1) J at an optimum pressure of 3.0 Torr with the corresponding efficiency of 0.18%.[2] The numerical experiment on this device was carried out using Lee model code to compute the optimum neon yield Y_{sxr} keeping the cathode radius b fixed at 3.2 cm, the anode length z_0 was drastically decreased from 16 cm to 7 cm, while the anode radius a was slightly increased from 0.95 cm to 1.2 cm from the standard configuration. As a result, the neon yield Y_{sxr} increased to 9.5 J at optimum pressure of 3.5 Torr with the corresponding efficiency of 0.32%.[13] This computed efficiency of neon yield Y_{sxr} got improved 2–3 times from the experimental value (0.18%) of the standard UNU/ICTP PFF.

Using the Lee model code, around 1994, Liu in his Ph.D. thesis[2] took an initiative to improve the yield of characteristic line X-ray from UNU/ICTP PFF.

One of the conclusions of his research work was that the reduction of L_0 down to 10 nH improved the percentage of stored energy (E_0) going into the plasma with a corresponding increase in Ne line yield.[2] This led to the design of a 16-Hz, 3-kJ, $L_0 = 12$ nH (best then possible) DPF built by AASC in the US, finally shipped and assembled at NIE. This machine[4] is now known as the NX2.

In this paper, the L_0 along with its corresponding electrode geometry (z_0, a and b) of the UNU/ICTP PFF machine is further optimized at 14 kV under different operating P_0 using the modified version of Lee model code to enhance the neon yield Y_{sxr}. Then neon yield Y_{sxr} are computed with our optimized combination of L_0, z_0, a and b at 11.5 kV and compared with the measured neon yield Y_{sxr} of the NX2 machine at 11.5 kV.

In this paper, Sec. 2 describes the Lee model code, whereas Sec. 3 describes the method of numerical experiment. The detailed description of numerical experiment for our optimization exercise is given in Sec. 4. Section 5 explains the process of finding optimum static inductance with its corresponding electrode configuration for possible maximum neon yield Y_{sxr} in our optimization.

2. Lee Model Code

The electrical circuit and plasma focus dynamics, thermodynamics (specific heat ratio and charge number as a function of temperature) and radiations are coupled by the "Lee model code" which enables a realistic simulation that helps analyze all of the gross properties and performances of a DPF machine.[18] This code is used in the interpretation of experiments and design of a DPF.[20] An improved five-phase code incorporating finite small disturbance speed, radiation and radiation-coupled dynamics was used[4] and was first published[21] in the Web in 2000. Plasma self-absorption was included[18,21] in 2007 improving the soft X-ray simulation with neon, argon and xenon among other gases. It has been widely used as a complementary facility in several machines, such as UNU/ICTP PFF,[4,12] NX1 and NX2[4] as well as DENA.[21] It has also been used in other machines for the design and interpretation including sub-kJ DPF machines,[22] FNII,[23] the UBA hard X-ray source,[24] KSU PF[25] and a cascading DPF.[26] Computed information from Lee model code includes axial and radial speeds and dynamics,[12,25] focus pinch duration and dimensions, average pinch temperatures and densities, soft X-ray characteristics and yield,[4,13] optimization of machines[4,12,13,18] and adaptation with modified Lee model code for Filipov-type DPF devices.[21] The modified six-phase version of the Lee model code RADPFV6.1b is developed for Type-2 (high-inductance DPF) machines which have been found to be incompletely fitted with the five-phase model due to a dominant anomalous resistance phase.[27]

In the Lee model code, the rate of neon line radiation is calculated as follows[18]:

$$\frac{dQ_L}{dt} = -4.6 \times 10^{-31} n_i^2 Z Z_n^4 (\pi r_p^2) z_{\max}/T\,, \tag{1}$$

where Q_L is the neon line radiation, Z_n is the atomic number, Z is the effective charge number, n_i is the number density, r_p the pinch radius, $z_{\max}$ is the pinch column length and T is the average temperature of pinch plasma. In the calculation of the code, Q_L is computed by integrating over the pinch duration. The neon yield Y_{sxr} must be equivalent to the line radiation yield, i.e. $Q_L = Y_{\text{sxr}}$, within the temperature window of 200–500 eV (2.32×10^6–5.8×10^6 K) which corresponds to an end axial speed of 6–7 cm/μs in the modified Lee model code.[2] Within this temperature range the ionization level of neon is such as to make it hydrogen-like or helium-like, so that the plasma emits the characteristic line radiation of neon.

3. Method of Numerical Experiment

The measured discharge current waveform is a significant indicator to realistically simulate and analyze all the gross performances of any DPF. Important information such as the axial and radial phase dynamics, temperature and thermodynamic properties, the crucial energy transfer into the focus pinch that causes nuclear fusion and hence the radiation yields from the device are quickly traced out from the current waveform.[20] This is why the discharge current waveform fitting is one of the best important techniques to optimize and configure a DPF. So, the fitting of the computed discharge current waveform to the measured current waveform through numerical experiment using Lee model code provides a lot of valuable insights of the pinched plasma.

First of all, the measured discharge current waveform is collected either from laboratory experiment or picked out from published literature. At the beginning of the numerical experiments, the code is configured for that DPF by providing the tube parameters, namely z_0, a and b; the bank parameters, namely the external static inductance L_0, capacitance of the capacitor bank C_0 and stray circuit resistance r_0; and the operating parameters, namely voltage V_0, P_0 and the fill gas.[1,20] Then, the computed total discharge current waveform is fitted to the measured waveform by sequential adjustment of the four model parameters: mass swept-up factor (f_m), plasma current factor (f_c) in the axial phase and accordingly the radial mass factor (f_{mr}) and radial current factor (f_{cr}) in the radial phase. During the first initiative of fitting, the values of axial model parameters f_m and f_c are adjusted in such a manner that the rising slopes of computed current waveform and peak discharge current are in reasonable agreement with the measured total current waveform. Then the radial model parameters f_{mr} and f_{cr} are varied until the computed slope deeply fits with the measured values.[1]

4. Numerical Experiments on UNU/ICTP PFF with Neon Filling Gas

To start the numerical experiments, the modified version of Lee model code (RADPFV5.15de) is configured for the UNU/ICTP PFF with the following published parameters[13]:

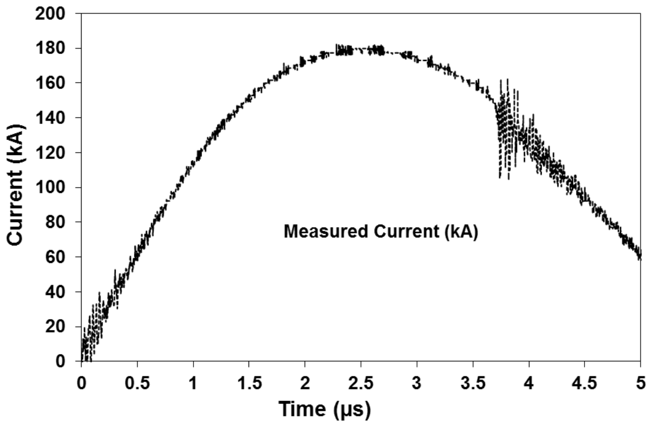

Fig. 1. Measured discharge current waveform of the UNU/ICTP PFF operated at 14 kV, 30 μF and 2.8 Torr with neon gas.

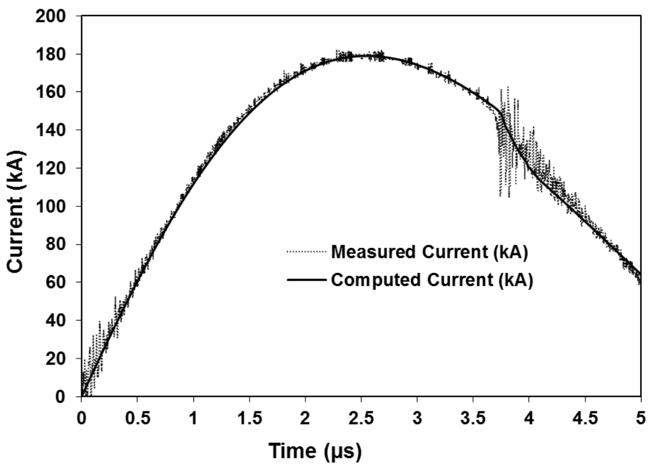

Fig. 2. Fitting of the measured current waveform (dotted line) with the computed current waveform (solid line) of UNU/ICTP PFF operated at 14 kV, 30 μF and 2.8 Torr with neon gas.

- Bank parameters: $L_0 = 110$ nH, $C_0 = 30$ μF and $r_0 = 12$ mΩ.
- Tube parameters: $b = 3.2$ cm, $a = 0.95$ cm and $z_0 = 16$ cm.
- Operating parameters: $V_0 = 14$ kV, neon gas (MW = 20, $A = 10$ and At-1 mol-2 = 1) and $P_0 = 2.8$ Torr.

A measured discharge current waveform of the UNU/ICTP PFF operated at 14 kV, 30 μF and 2.8 Torr with neon gas has been collected from the published waveform (see Ref. 28), presented in Fig. 1.

A reasonably good adjustment (Fig. 2) of the computed total discharge current waveform with the measured current waveform has been obtained with the following model parameters[13]: $f_m = 0.05$, $f_c = 0.7$, $f_{mr} = 0.2$ and $f_{cr} = 0.8$.

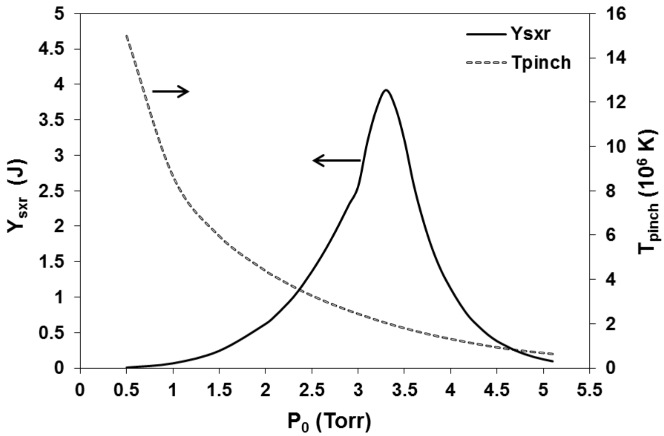

Fig. 3. Computed neon yields $Y_{\rm sxr}$ and the pinched plasma temperatures with respect to pressure of UNU/ICTP PFF operating at 14 kV and 30 μF.

These fitted values of the model parameters are kept constant in all of our present numerical experiments for this paper.

The effects of P_0 on neon yield $Y_{\rm sxr}$ emission from the device have been observed keeping fixed all of the above-mentioned bank, tube and operating parameters.[13] In these numerical experiments, the pressure was varied in the range of 1.0–5.2 Torr and computed results are presented in Fig. 3.

From Fig. 3, it is observed that the neon yield $Y_{\rm sxr}$ increases with increasing gas pressure until it reaches the maximum value of about 3.92 J at $P_0 = 3.3$ Torr with the corresponding efficiency of 0.13% after which it decreases with further increase of the pressure.

At this optimum pressure ($P_0 = 3.3$ Torr), the computed end axial speed is $v_a = 5.4$ cm/μs, the total peak discharge current is $I_{\rm peak} = 180$ kA, the pinch current is $I_{\rm pinch} = 103$ kA and the focusing time is about 3.97 μs. It is also noticed that the focusing time increases with increasing P_0. This is because higher the gas pressure, lower the current sheath (CS) velocity in both axial and radial phases and hence the focus time becomes slower with increase in gas pressure.

The characteristics of the variation of neon yield $Y_{\rm sxr}$ with pressure depend on two major factors that are given below:

- First, at the computed optimum P_0, the v_a of CS is about 5.4 cm/μs, which corresponds to the pinch temperature of 2.04×10^6 K. This temperature is very close to the correct pinch temperature window for the optimum neon yield $Y_{\rm sxr}$ emission.[29]
- Second, the radiation yield is proportional to the square of the plasma density. When the pressure is increased from a low value, the density of the pinched radiating plasma increases and as a result the X-ray emission increases. Thus, at

very low pressure the pinch plasma density is too low while the pinch temperature is very high due to high CS velocity. On the other hand, at very high pressure the pinch plasma density would be high and also the corresponding pinch temperature will be too low because of low CS velocity. In both cases, the pinch temperature may be away from the temperature window and hence the emitted neon yield Y_{sxr} is low.

Therefore, there would be an optimum pressure at which the pinch temperature and the corresponding end axial CS velocity are within the expected range while the density is still high enough for getting the maximum neon yield Y_{sxr} as shown in Fig. 3.

The measured values of neon yield Y_{sxr} from UNU/ICTP PFF have been obtained by Liu[2] using a five-channel PIN soft X-ray detector confirmed by a calorimeter. In this experiment, the maximum value of neon yield Y_{sxr} from this device was found to be about (5.4 ± 1) J at the optimum pressure of $P_0 = 3.0$ Torr with the corresponding efficiency of 0.18%. At this optimum P_0, the typical values are as follows: end axial speed is $v_a = 5.7$ cm/μs, the total peak discharge current is $I_{\mathrm{peak}} = 180$ kA and the pinch current is $I_{\mathrm{pinch}} = 111$ kA.

In addition, many numerical experiments have been carried out to observe the effect of applied voltage on the neon yield Y_{sxr} from UNU/ICTP PFF versus the pressure. The variations of neon yield Y_{sxr} with pressure from this device are plotted at applied voltages of 12, 13, 14 and 15 kV as shown in Fig. 4.

From Fig. 4, it is observed that at optimum P_0, the neon yield Y_{sxr} rises from 2.74 J to 4.49 J with increasing the applied voltage from 12 kV to 15 kV. It is also noticed that for all applied voltages, the general nature of variations of neon yield Y_{sxr} with pressure is almost the same, but the optimum pressure values shift to higher ones with increasing the operating voltages.

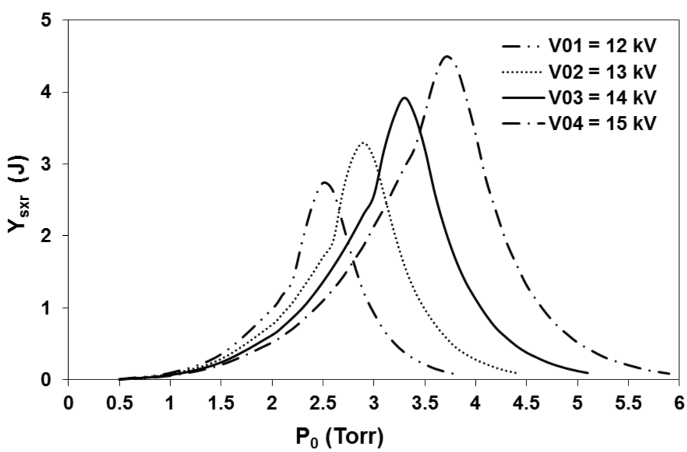

Fig. 4. Variations of computed neon yield Y_{sxr} from UNU/ICTP PFF versus pressure at different operating voltages.

The anode geometry (a and z_0) along with the operating P_0 of UNU/ICTP PFF has also been optimized through numerical experiments using the Lee model code, keeping fixed b at its standard value of 3.2 cm for enhancing the neon yield Y_{sxr}.[3] During this practical optimization, z_0 is reduced drastically from 16 cm to 7 cm; a is increased from 0.95 cm to 1.2 cm. During this optimum anode configuration, the computed values are: $v_a = 4.9$ cm/μs, $I_{\text{peak}} = 184$ kA, $I_{\text{pinch}} = 141$ kA and the neon yield Y_{sxr} is about 9.5 J at an optimum $P_0 = 3.5$ Torr with the corresponding efficiency of 0.32%. It is found from these observations that the neon yield Y_{sxr} (9.5 J) at the optimum combination of a, z_0 and P_0 increases 2–3 times from the measured value (5.4 ± 1 J) at the optimum P_0 of standard UNU/ICTP PFF configuration. It this case the corresponding I_{pinch} also increases from 111 kA (typical value) to 141 kA (computed).

It is noticed that with only pressure optimization of the machine, the computed neon yield Y_{sxr} (3.92 J) at the optimum pressure decreases from both the measured value and the value after a and z_0 optimization, while I_{pinch} reduces to 103 kA. Therefore, it may be concluded that enhancing the neon yield Y_{sxr} by further increasing I_{pinch} is found to be a suitable technique. In the next section, we will discuss the technique for increasing I_{pinch} along with improving the neon yield Y_{sxr}.

5. Optimization of L_0 Along with Electrode Geometry at Different P_0

At the standard configuration of UNU/ICTP PFF device, the reduction effects of L_0 on discharge current waveforms with time are observed through numerical experiments at $P_0 = 3.3$ Torr of neon gas. The computed results are presented in Fig. 5.

It is found from Fig. 5 that I_{peak} comes earlier and also its value increases for each reduction of L_0, consequently I_{pinch} will increase. For example, when $L_0 =$

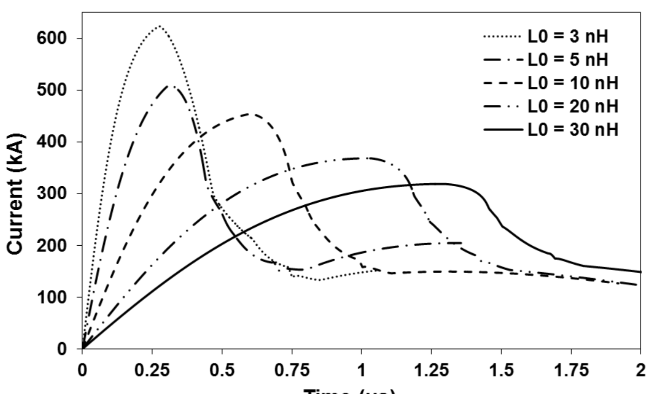

Fig. 5. Computed discharge current waveforms as a function of time for operation at 14 kV, 30 μF, $P_0 = 3.3$ Torr of neon for operation with different values of L_0.

30 nH, $I_{\rm peak} = 318.45$ kA at 1.28 μs, when $L_0 = 20$ nH, $I_{\rm peak} = 368.11$ kA at 1.02 μs, when $L_0 = 10$ nH, $I_{\rm peak} = 453.91$ kA at 0.60 μs, when $L_0 = 5$ nH, $I_{\rm peak} = 508.44$ kA at 0.31 μs and when $L_0 = 3$ nH, $I_{\rm peak} = 623.21$ kA at 0.28 μs. Therefore, neon yield $Y_{\rm sxr}$ can be improved by reducing L_0 from its value of 30 nH.

To compute the optimum L_0 together with its corresponding optimum combination of z_0, a and b for improving the neon yield $Y_{\rm sxr}$ from the optimized UNU/ICTP PFF, the values of $V_0 = 14$ kV and $C_0 = 30$ μF are kept constant throughout the present numerical experiments. We compute six sets of optimum configurations of z_0, a, b and L_0 at six operating $P_0 = 2.0$, 2.5, 3.3, 4.0, 5.0 and 6.0 Torr, respectively. Because, our aim is to find an optimum combination of z_0, a, b and L_0 and also investigate the effect of operating pressure P_0 on the neon yield $Y_{\rm sxr}$ for improving it.

In these numerical experiments, for each value of L_0 the corresponding r_0 is computed, so that the factor RESF [RESF = stray circuit resistance/surge impedance; $r_0/\sqrt{(L_0/C_0)}$] remains unchanged at 0.2. Again, for each L_0 the values of a and b are adjusted in such a manner that their ratio ($c = b/a$) remains at a constant value of 3.368 (Ref. 16) and L_0 was varied from 110 nH to 3 nH at each operating pressure P_0.

The following procedure is applied to get the optimum combination of L_0, z_0, a and b at each operating pressure P_0 for getting an improved value of neon yield $Y_{\rm sxr}$ (Ref. 16):

(i) The value of P_0 is kept constant at a certain value for all values of L_0 and also the value of z_0 is fixed at a certain value for each L_0.
(ii) Then a and correspondingly b are varied keeping $c = 3.368$, until the maximum neon yield $Y_{\rm sxr}$ is computed for a certain value of z_0.
(iii) Then a and correspondingly b are varied keeping $c = 3.368$, until the maximum neon yield $Y_{\rm sxr}$ is computed for a certain value of z_0.
(iv) Also a as well as b are varied with different values of z_0 at each L_0 to obtain the optimum combination for the maximum neon yield $Y_{\rm sxr}$.
(v) After that another value of z_0 is chosen, the maximum neon yield $Y_{\rm sxr}$ is computed by varying a and b and so on, until we have the optimum combination of z_0, a and b for the best improved neon yield $Y_{\rm sxr}$ at a fixed value of L_0.
(vi) The above procedure is repeated with gradually reducing L_0 until it reached 3 nH.
(vii) Then another value of P_0 is taken and the procedure in (i)–(v) is followed carefully to compute the optimum combination of z_0, a and b for the best improved neon yield $Y_{\rm sxr}$ at each value of L_0 and so on.

Since the time taken by the plasma CS to reach the anode end needs to coincide with the rising time of $I_{\rm peak}$ for the maximum energy transfer to the crucial pinch region, z$_0$ needs to be reduced with the reduction of L_0 for time matching as $I_{\rm peak}$ comes earlier, as illustrated in Fig. 5. At the same time, because of reducing L_0, the value of $I_{\rm peak}$ increases as a result a as well as b were necessarily increased

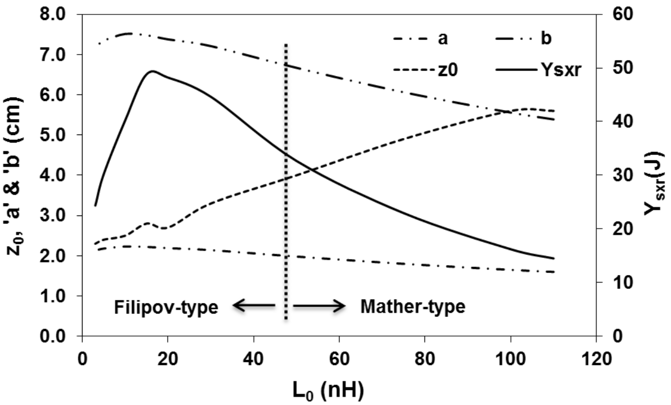

Fig. 6. Computed values of yield Y_{sxr} and its corresponding optimum electrode geometry with respect to L_0 at 14 kV, 30 μF and 2.0 Torr with neon gas.

leading to longer pinch length ($z_{\max}$) and hence a bigger pinch inductance [$L_p = (\mu/2\pi) \times \ln(b/r_p) \times z_{\max}$] is found. Thus, the geometry of the machine moved from a longer and thinner (Mather-type) one to shorter and fatter (Filipov-type) one, as shown in Fig. 6. As L_p increases with decreasing L_0, the dynamic pinch inductive load increases.

The values of a as well as b are varied with different values of z_0 at each L_0 to compute the optimum combination of them for getting the maximum neon yield Y_{sxr}, which corresponds closely to the largest I_{pinch}. The computed maximum possible values of neon yield Y_{sxr} along with the corresponding efficiencies at $P_0 = 2.0$ Torr for each L_0 and the corresponding optimum combinations of z_0, a and b are presented in Table 1.

Table 1 shows that as L_0 is reduced, I_{peak} increases and at each reduction of L_0 the corresponding I_{peak} is larger than the previous value. This occurs continuously without showing any sign of limitation as a function of L_0. Whereas, I_{pinch} also

Table 1. The optimum combination of z_0, a and b at each value of L_0 with the corresponding neon yield Y_{sxr} at fixed $c = b/a = 3.368$, $P_0 = 2.0$ Torr, $V_0 = 14$ kV, $C_0 = 30$ μF, RESF = 0.2, $f_m = 0.05$, $f_c = 0.7$, $f_{\mathrm{mr}} = 0.2$ and $f_{\mathrm{cr}} = 0.8$.

L_0 (nH)	z_0 (cm)	b (cm)	a (cm)	I_{peak} (kA)	I_{pinch} (kA)	T_{pinch} ($\times 10^6$ K)	v_a (cm/μs)	$a_{\min}$ (cm)	$z_{\max}$ (cm)	Y_{sxr} (J/shot)	Efficiency (%Y_{sxr})
110	5.60	5.389	1.60	182.65	137.16	2.0	4.071	0.093	2.348	14.51	0.49
100	5.60	5.557	1.65	191.15	142.01	2.0	4.156	0.096	2.425	16.22	0.55
75	4.90	6.062	1.80	216.52	156.25	2.0	4.304	0.106	2.675	22.94	0.78
50	4.00	6.669	1.98	255.34	174.99	2.1	4.585	0.125	2.962	32.66	1.11
30	3.30	7.208	2.14	310.23	194.55	2.2	5.148	0.152	3.267	44.62	1.52
25	2.50	7.208	2.14	318.40	196.8	2.3	5.149	0.159	3.305	45.25	1.54
20	2.70	7.376	2.19	351.73	204.16	2.4	5.672	0.178	3.419	48.19	1.64
15	**2.80**	**7.477**	**2.22**	**390.63**	**209.85**	**2.4**	**6.322**	**0.2**	**3.515**	**48.83**	**1.66**
10	2.50	7.511	2.23	436.18	212.59	2.5	7.077	0.241	3.501	40.26	1.37
5	2.40	7.342	2.18	506.85	211.12	2.5	8.694	0.288	3.463	30.28	1.03
3	2.30	7.174	2.13	543.64	206.43	2.6	9.762	0.308	3.379	24.35	0.83

increases gradually with reduction of L_0 and finally it reaches a maximum value of 212.59 kA at $L_0 = 10$ nH, then it starts to decrease and also the ratio of $I_{\mathrm{pinch}}/I_{\mathrm{peak}}$ drops progressively with further reduction of L_0. Thus, I_{peak} does not show any limitation of increment while I_{pinch} has a maximum value as L_0 is progressively reduced. This pinch current limitation effect is not a simple one.

The following three reasons make the combined effect that limits I_{pinch} current:

(i) If L_0 is reduced to zero then I_{peak} would not be infinity because at $L_0 = 0$ though the surge impedance $Z_0 = \sqrt{(L_0/C_0)}$ is zero, the dynamics of plasma CS produces an impedance[30,31] which then becomes the dominating load to limit the value of I_{peak}.

(ii) The capacitor bank will discharge within a short time through the focus pinch as L_0 is reduced to a very small value and it becomes more and more immediately coupled to the pinch.

(iii) For the energy distributions and the requirement to adjust z_0, a as well as b, the situation requires that as L_0 is decreased, the ratio of $I_{\mathrm{pinch}}/I_{\mathrm{peak}}$ reduces.[32]

Looking at Table 1, it is also observed that as L_0 is reduced gradually, there is a corresponding increase in a as well as b, whereas z_0 decreased progressively.

In addition, for each reduction of L_0, the plasma pinch dimensions (pinch radius a_{min} and pinch length z_{max}) increase as a result the neon yield Y_{sxr} increases [refer Eq. (1)]. From this table, it can be noticed that the neon yield Y_{sxr} increases as L_0 is reduced with its corresponding optimum combination of z_0, a and b. This happens until the neon yield Y_{sxr} reaches a maximum value of 48.83 J with the corresponding efficiency of 1.16% at $L_0 = 15$ nH and corresponding combination of $z_0 = 2.8$ cm, $a = 2.2$ cm and $b = 7.477$ cm, beyond which the neon yield Y_{sxr} does not increases with further reduction of L_0. Therefore, this is an optimum configuration of UNU/ICTP PFF machine operating at $P_0 = 2.0$ Torr. At this optimized configuration the computed value of neon yield Y_{sxr} (48.83 J) is about 10 times higher than that of the measured value (5 ± 1 J). The bold text in Table 1 indicates the optimized values of z_0, a, b and L_0 along with the corresponding neon yield Y_{sxr} and efficiency. The variations of optimum neon yield Y_{sxr} and its corresponding optimum combination of z_0, a and b with L_0 are shown in Fig. 6. This figure shows that neon yield Y_{sxr} increases with reduction of L_0 and after a certain minimum value of L_0, neon yield Y_{sxr} starts to decrease. From the careful observation of this figure, it is seen that the optimum values of a and b gradually increase, whereas z_0 proportionally decreases with each reduction of L_0.

Since our motivation is to improve neon yield Y_{sxr} from UNU/ICTP PFF by computing the optimized combination of z_0, a and b for each L_0 (from 110 nH to 3 nH), we carry out a lot of numerical experiments at other five operating P_0 (i.e. 2.5, 3.3, 4.0, 5.0 and 6.0 Torr) following a similar procedure as discussed above. From the computed results, it is observed that the values of I_{peak}, I_{pinch} and Y_{sxr} increase for each reduction of L_0 along with its corresponding optimum combination of z_0, a and b at each operating pressure P_0.

Table 2. The optimum combinations of z_0, a, b and L_0 at an operating pressure of $P_0 = 4.0$ Torr with their corresponding neon yield Y_{sxr} at fixed $c = b/a = 3.368$, $V_0 = 14$ kV, $C_0 = 30$ μF, RESF = 0.2, $f_m = 0.05$, $f_c = 0.7$, $f_{mr} = 0.2$ and $f_{cr} = 0.8$.

L_0 (nH)	z_0 (cm)	b (cm)	a (cm)	I_{peak} (kA)	I_{pinch} (kA)	T_{pinch} ($\times 10^6$ K)	v_a (cm/μs)	$a_{\min}$ (cm)	$z_{\max}$ (cm)	Y_{sxr} (J/shot)	Efficiency (%Y_{sxr})
110	6.60	3.738	1.11	184.01	140.04	2.16	4.27	0.07	1.61	8.35	0.28
100	6.20	3.873	1.15	191.89	145.26	2.17	4.29	0.07	1.66	9.38	0.32
75	5.10	4.244	1.26	216.86	161.21	2.22	4.37	0.08	1.83	13.46	0.46
50	4.40	4.850	1.44	258.78	183.27	2.20	4.59	0.10	2.13	21.34	0.73
30	3.60	5.389	1.60	316.99	207.74	2.29	5.06	0.11	2.41	34.22	1.16
25	3.30	5.591	1.66	338.83	214.25	2.26	5.20	0.12	2.53	39.39	1.34
20	2.90	5.726	1.70	364.21	221.25	2.30	5.43	0.13	2.62	45.24	1.54
15	2.50	5.793	1.72	395.88	227.61	2.38	5.81	0.14	2.71	52.67	1.79
10	**2.10**	**5.759**	**1.71**	**438.88**	**231.95**	**2.50**	**6.48**	**0.15**	**2.77**	**57.16**	**1.94**
5	2.35	5.726	1.70	523.17	235.80	2.61	8.16	0.19	2.72	46.24	1.57
3	2.34	5.625	1.67	564.54	232.08	2.62	9.17	0.21	2.65	38.07	1.29

At each P_0, the increment of I_{peak} has no limit with the reduction of L_0 while at a certain value of L_0, I_{pinch} achieves a maximum value and then starts to reduce for further decrease of L_0 due to pinch current limitation effect. It is observed that in the optimization of z_0, a and b with L_0 of UNU/ICTP PFF operating at $P_0 = 2.0$, 2.5 and 3.3 Torr, the computed maximum neon yield Y_{sxr} is found at $L_0 = 15$ nH.

From Table 2, it is observed that the optimum combination of $z_0 = 2.10$ cm, $a = 1.71$ cm and $b = 5.759$ cm is obtained at $L_0 = 10$ nH when it is operated at $P_0 = 4.0$ Torr and at this configuration the computed maximum neon yield Y_{sxr} is found to be 57.16 J with a corresponding efficiency of 1.94%.

Here, the optimum L_0 is lower than our previously computed optimum value at a lower operating pressure. The bold text in Table 2 shows the optimum results. This computed value is about 11–12 times higher than the measured value (5 ± 1 J).

Similarly, at $P_0 = 5.0$ Torr and 6.0 Torr, the optimum combinations of z_0, a and b of UNU/ICTP PFF are obtained at $L_0 = 10$ nH with the maximum neon yield Y_{sxr}.

The summarized results of optimization of L_0, z_0, a and b of UNU/ICTP PFF at six operating pressures P_0 are presented in Table 3.

From Table 3, the effect of P_0 on optimization of z_0, a, b and L_0 can be analyzed as follows:

- From this table, it is found that at each P_0 the optimum neon yield Y_{sxr} is found to be almost constant at $v_a \sim 6.2$ cm/μs and the corresponding maximum pinch temperature T_{pinch} ($\sim 2.4 \times 10^6$ K) is also constant. This value of T_{pinch} is very close to the temperature window of neon plasma for radiating maximum soft X-ray. So, these computed neon yield Y_{sxr} are reasonably good.
- It is also observed from this table that at lower P_0 (say 2.0, 2.5 and 3.3 Torr), each optimum combination of z_0, a and b is found at $L_0 = 15$ nH for which the maximum neon yield Y_{sxr} is obtained, but for higher P_0 (say 4.0, 5.0 and 6.0 Torr) the maximum yield is found at $L_0 = 10$ nH. Technically, it is difficult and

Table 3. The optimum combinations of z_0, a, b and L_0 at six operating pressures $P_0 = 2.0$, 2.5, 3.3, 4.0, 5.0 and 6.0 Torr with their corresponding neon yield $Y_{\rm sxr}$ at fixed $c = b/a = 3.368$, $V_0 = 14$ kV, $C_0 = 30$ μF, RESF = 0.2, $f_m = 0.05$, $f_c = 0.7$, $f_{mr} = 0.2$ and $f_{cr} = 0.8$.

P_0 (Torr)	L_0 (nH)	z_0 (cm)	b (cm)	a (cm)	$I_{\rm peak}$ (kA)	$I_{\rm pinch}$ (kA)	$T_{\rm pinch}$ ($\times 10^6$ K)	v_a (cm/μs)	$a_{\rm min}$ (cm)	$z_{\rm max}$ (cm)	$Y_{\rm sxr}$ (J/shot)	Efficiency (%$Y_{\rm sxr}$)
2.0	15	2.8	7.477	2.22	390.63	209.85	2.40	6.322	0.2	3.515	48.83	1.66
2.5	15	1.9	6.702	1.99	368.25	209.62	2.41	5.71	0.16	3.18	51.23	1.74
3.3	**15**	**3.0**	**6.231**	**1.85**	**400.49**	**223.78**	**2.41**	**6.13**	**0.15**	**2.91**	**54.60**	**1.86**
4.0	10	2.1	5.759	1.71	438.88	231.95	2.50	6.48	0.15	2.77	57.16	1.94
5.0	10	2.5	5.389	1.60	453.32	241.31	2.47	6.53	0.14	2.58	56.32	1.92
6.0	10	2.6	5.018	1.49	456.89	247.71	2.50	6.49	0.13	2.39	52.43	1.78

Table 4. The comparison of neon yield $Y_{\rm sxr}$ for our optimization and the experimental NX2 at various operating P_0 and $V_0 = 11.5$ kV, $f_m = 0.05$, $f_c = 0.7$, $f_{mr} = 0.2$ and $f_{cr} = 0.8$.

Machine	P_0 (Torr)	L_0 (nH)	z_0 (cm)	B (cm)	a (cm)	$I_{\rm peak}$ (kA)	I_D (kA $\cdot$ cm^{-1})	SF (kA $\cdot$ cm^{-1} Torr^{-1})	$Y_{\rm sxr}$ (J)	Efficiency (%$Y_{\rm sxr}$)
Our optimization	2.0	15	2.80	7.477	2.22	338.16	152.32	107.71	22.13	1.11
	2.5	15	1.90	6.702	1.99	321.92	161.77	102.31	26.87	1.35
	3.3	**15**	**3.00**	**6.231**	**1.85**	**343.73**	**185.80**	**102.28**	**29.05**	**1.46**
	4.0	10	2.10	5.759	1.71	383.52	224.28	112.14	31.63	1.59
	5.0	10	2.5	5.389	1.6	392.03	245.02	109.58	34.38	1.73
	6.0	10	2.6	5.018	1.49	393.82	264.31	107.90	33.99	1.71
Experimental NX2	1.5	15	7.0	4.0	1.9	340	170	139	7.0	0.38
	3.0	**15**	**5.0**	**4.0**	**1.9**	**400**	**200**	**115**	**18.0**	**0.97**
	5.25	15	4.0	4.0	1.9	410	205	90	15.0	0.81

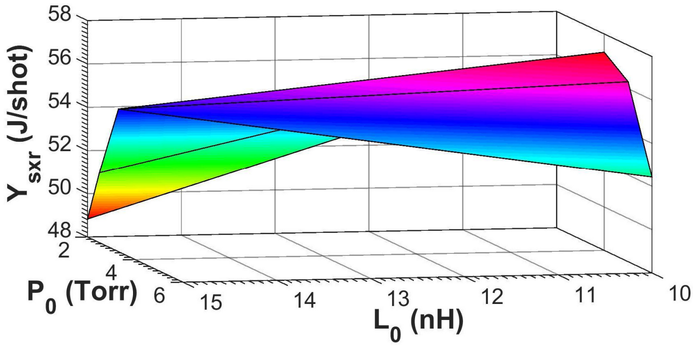

Fig. 7. A 3D plot of optimum neon $Y_{\rm sxr}$ versus optimum L_0 at six operating P_0 for our optimization at 14 kV and 30 μF.

expensive to have a capacitor bank with inductance less than 15 nH. Therefore, the optimization of z_0, a, b and L_0 is good at lower P_0.

- This table shows that the minimum pinch column radius ($a_{\rm min}$) is almost constant at ~ 0.16 cm and its maximum length ($z_{\rm max}$) varies in the range of $\sim$ (3.5–2.4 cm) at each optimum combination of z_0, a, b and L_0 for each P_0. At the optimum combination of z_0, a, b and L_0 for each P_0, the $z_{\rm max}$ gets its maximum value than all other optimum combinations of them. It is clear from Eq. (1) that neon yield $Y_{\rm sxr}$ is directly proportional to $z_{\rm max}$. So, it is one of the important reasons for getting maximum neon yield $Y_{\rm sxr}$ at the optimum combination of z_0, a, b and L_0.
- In addition, it is noticed that the optimum values of both a and b decrease with increase of P_0.

A correlation among the optimum neon Y_{xsr} yield and L_0 at six operating P_0 of our optimization is depicted by a three-dimensional plot which is illustrated in Fig. 7. Figure 7 shows that neon $Y_{\rm sxr}$ yield rises proportionally with increasing P_0 from its lower value keeping fixed L_0 at 15 nH, whilst after a certain value of P_0, neon $Y_{\rm sxr}$ yield starts to reduce remaining constant L_0 at 10 nH. The maximum value of neon $Y_{\rm sxr}$ yield is found at higher P_0 but at low L_0. From the comparison of the computed neon $Y_{\rm sxr}$ yield from Fig. 7 with the measured one (Ref. 2), from the comparison of the results (from Table 3), it is found that the variation trend of computed neon yield $Y_{\rm sxr}$ with P_0 at different optimized configurations of z_0, a, b and L_0 of UNU/ICTP PFF is similar with the measured neon yield $Y_{\rm sxr}$ at different P_0 of the standard of UNU/ICTP PFF.[2] The maximum measured neon yield $Y_{\rm sxr}$ (5 ± 1 J) has been found at the optimum $P_0 = 3.0$ Torr for the standard machine, while the maximum computed value of it (57.2 J) is obtained at an operating pressure $P_0 = 4.0$ Torr for our optimized configuration and then neon yield $Y_{\rm sxr}$ drops on both sides of this P_0. This maximum computed value of neon yield $Y_{\rm sxr}$ for optimized configuration is about 11–12 times higher than the measured value for the standard machine.

In addition, using the modified Lee model code, neon yield $Y_{\rm sxr}$ of our optimized configuration is computed at each P_0 and $V_0 = 11.5$ kV keeping fixed the minimum pinch temperature ($T_{\rm pinch\_min}$) within the temperature window of neon gas (around 1.9×10^6 K) by merely adjusting f_{mr} and the computed results are presented in Table 4. The measured neon yield $Y_{\rm sxr}$ of NX2 machine at $P_0 = 1$–5 Torr and $V_0 = 11.5$ kV have been collected[4,33] and placed in this table.

From Table 4, it is found that the speed factor (SF) at each optimum configuration of z_0, a, b and L_0 is nearly constant (∼102). The constancy and similarity of SF to its standard value justify the computed results in Table 4. The maximum measured neon yield $Y_{\rm sxr}$ (18 J) was found at 3 Torr and $z_0 = 5$ cm. In our optimization, each optimum value of z_0 is lower than that of the standard NX2. It is observed from Table 4 that the neon yield $Y_{\rm sxr}$ with the corresponding efficiencies of our optimized machine are higher than those of NX2.

Based on the obtained results of these sets of numerical experiments with neon gas, it can be said that to improve the neon yield $Y_{\rm sxr}$, L_0 should be reduced to a value around 15–20 nH, which is an achievable range incorporating low-inductance technology, below which the pinch current $I_{\rm pinch}$, the yield $Y_{\rm sxr}$ as well as the corresponding efficiency would not be improved significantly, if at all. Moreover, the neon yield $Y_{\rm sxr}$ may be improved 11–12 times from the standard UNU/ICTP PFF value by a remarkable increase in b and a with reducing z_0 and L_0, keeping $c = b/a$ constant at 3.368 in the laboratory. In addition, significant reduction of z_0 and slightly increase in b from the standard NX2, the neon yield $Y_{\rm sxr}$ is also enhanced.

6. Conclusions

The Lee model code (RADPFV5.15de) is applied to characterize and optimize the UNU/ICTP PFF operated at 14 kV and 30 μF as a source of neon yield $Y_{\rm sxr}$. The reduction effects of L_0 along with its corresponding optimum combination of z_0, a and b on the neon yield $Y_{\rm sxr}$ at six operating pressures P_0 are investigated through a lot of numerical experiments. The limitation effect of L_0 on neon yield $Y_{\rm sxr}$ is also observed from these numerical experiments. It is observed that with the optimization of L_0, z_0, a and b, the optimum neon yield $Y_{\rm sxr}$ increases with increasing P_0 up to 4.0 Torr and then it starts to decrease with further increasing P_0. The computed neon yield $Y_{\rm sxr}$ from the optimized machine at different P_0 vary in the range of 48.83–57.16 J which is 10–11 times higher than the experimentally measured value (5.4 ± 1 J) of the standard UNU/ICTP PFF. At $P_0 = 4.0$ Torr, the maximum neon yield $Y_{\rm sxr}$ (57.2%) is obtained at $L_0 = 10$ nH. Though, at higher operating P_0, the optimum neon yield $Y_{\rm sxr}$ shows higher value but L_0 gets to such low values that are difficult to achieve practically. Therefore, the best optimum combination of $L_0 = 15$, $z_0 = 3.0$ cm, $a = 1.85$ cm and $b = 6.231$ cm is computed at $P_0 = 3.3$ Torr and then the optimum neon yield $Y_{\rm sxr}$ is found to be 54.6 J with the corresponding efficiency of 1.86%. Finally, our obtained optimized configuration through numerical experiments may be used to design a new device to have better soft X-ray yield than both the UNU/ICTP PFF and NX2.

References

1. S. Lee, S. H. Saw, L. Soto, S. V. Springham and S. P. Moo, *Plasma Phys. Contr. Fusion* **51** (2009) 075006.
2. M. Liu, Soft X-rays from compact plasma focus, Ph.D. thesis, Nanyang Technological University (1996).
3. M. Habibi, R. Amrollahi and G. R. Etaati, *J. Fusion Energy* **29** (2010) 49.
4. S. Lee, P. Lee, G. Zhang, X. Feng, V. A. Gribkov, M. Liu and T. K. Wong, *IEEE T. Plasma Sci.* **26** (1998) 1119.
5. A. D. Cahill, D. A. Hammer, S. A. Pikuz and T. A. Shelkovenko, *Rev. Sci. Instrum.* **87** (2016) 107101.
6. S. M. Hassan and P. Lee, in *Plasma Science and Technology for Emerging Economies* (Springer, Singapore, 2017), pp. 269–292.
7. A. Depresseux, E. Oliva, J. Gautier, F. Tissandier, J. Nejdl, M. Kozlova and H. T. Kim, *Nat. Photonics* **9** (2015) 817.
8. J. Miao, T. Ishikawa, I. K. Robinson and M. M. Murnane, *Science* **348** (2015) 530.
9. S. Hussain, M. Shafiq, R. Ahmad, A. Waheed and M. Zakaullah, *Plasma Sources Sci. Technol.* **14** (2005) 61.
10. F. N. Beg, I. Ross, A. Lorenz, J. F. Worley, A. E. Dangor and M. G. Haines, *J. Appl. Phys.* **88** (2000) 3225.
11. V. A. Gribkov, A. Srivastava, P. L. C. Keat, V. Kudryashov and S. Lee, *IEEE T. Plasma Sci.* **30** (2002) 1331.
12. S. Lee, T. Y. Tou, S. P. Moo, M. A. Eissa, A. V. Gholap, K. H. Kwek and M. Zakaullah, *Am. J. Phys.* **56** (1988) 62.
13. S. H. Saw, P. C. K. Lee, R. S. Rawat and S. Lee, *IEEE T. Plasma Sci.* **37** (2009) 1276.
14. M. Zakaullah, K. Alamgir, M. Shafiq, M. Sharif, A. Waheed and G. Murtaza, *J. Fusion Energy* **19** (2000) 143.
15. S. Lee, S. H. Saw, P. Lee and R. S. Rawat, *Plasma Phys. Contr. Fusion* **51** (2009) 105013.
16. S. Al-Hawat, M. Akel and S. Lee, *J. Fusion Energy* **30** (2011) 494.
17. S. Lee and A. Serban, *IEEE T. Plasma Sci.* **24** (1996) 1105.
18. S. Lee, Radiative Dense Plasma Focus Computation Package: RADPF (2014), http://www.plasmafocus.net [see also http://www.intimal.edu.my/school/fas/UFLF/File1RADPF.htm (archival website)].
19. S. Lee and S. H. Saw, The plasma focus-numerical experiments, insights and applications in R. S. Rawat (ed.), *Plasma Science and Technology for Emerging Economies* (Springer Nature Singapore Pte Ltd., 2017), doi:10.1007/978-981-10-4217-1-3.
20. S. Lee, *J. Fusion Energy* **33** (2014) 319.
21. V. Siahpoush, M. A. Tafreshi, S. Sobhanian and S. Khorram, *Plasma Phys. Control. Fusion* **47** (2005) 1065.
22. L. Soto, P. Silva, J. Moreno, G. Silvester, M. Zambra, C. Pavez and W. Kies, *Braz. J. Phys.* **34** (2004) 1814.
23. H. Acuna, F. Castillo, J. Herrera and A. Postal, in *Proc. Int. Conf. Plasma Science* (1996), p. 127.
24. C. Moreno, V. Raspa, L. Sigaut, R. Vieytes and A. Clausse, *Appl. Phys. Lett.* **89** (2006) 091502.
25. A. E. Abdou, M. I. Ismail, A. E. Mohamed, S. Lee, S. H. Saw and R. Verma, *IEEE T. Plasma Sci.* **40** (2012) 2741.
26. S. Lee, *IEEE T. Plasma Sci.* **19** (1991) 912.
27. S. Lee, S. H. Saw, A. E. Abdou and H. Torreblanca, *J. Fusion Energy* **30** (2011) 277.

28. INTI International University, UNU/ICTP PFF (2017), http://www.intimal.edu.my/school/fas/UFLF/machines/UNU.htm.
29. S. Bing, Plasma dynamics and X-ray emission of the plasma focus, Ph.D. thesis, Nanyang Technological University (2000).
30. S. Lee, *Plasma Phys. Contr. Fusion* **50** (2008) 105005.
31. S. Lee, *Appl. Phys. Lett.* **95** (2009) 151503.
32. S. Lee and S. H. Saw, *Appl. Phys. Lett.* **92** (2008) 021503.
33. P. Gautam, R. Khanal, S. H. Saw and S. Lee, *J. Fusion Energy* **34** (2015) 686.